

Article

# Selective Catalytic Oxidation of Lean-H<sub>2</sub>S Gas Stream to Elemental Sulfur at Lower Temperature

Daniela Barba , Vincenzo Vaiano  and Vincenzo Palma 

Department of Industrial Engineering, University of Salerno, Via Giovanni Paolo II, 132, 84084 Fisciano, Italy; vvaiano@unisa.it (V.V.); vpalma@unisa.it (V.P.)

\* Correspondence: dbarba@unisa.it

**Abstract:** Ceria-supported vanadium catalysts were studied for H<sub>2</sub>S removal via partial and selective oxidation reactions at low temperature. The catalysts were characterized by N<sub>2</sub> adsorption at 77 K, Raman spectroscopy, X-ray diffraction techniques, and X-ray fluorescence analysis. X-ray diffraction and Raman analysis showed a good dispersion of the V-species on the support. A preliminary screening of these samples was performed at fixed temperature ( $T = 327\text{ }^{\circ}\text{C}$ ) and H<sub>2</sub>S inlet concentration (10 vol%) in order to study the catalytic performance in terms of H<sub>2</sub>S conversion and SO<sub>2</sub> selectivity. For the catalyst that exhibited the higher removal efficiency of H<sub>2</sub>S (92%) together with a lower SO<sub>2</sub> selectivity (4%), the influence of temperature (307–370 °C), contact time (0.6–1 s), and H<sub>2</sub>S inlet concentration (6–15 vol%) was investigated.

**Keywords:** hydrogen sulfide; H<sub>2</sub>S selective partial oxidation; sulfur; sulfur dioxide; vanadium-based catalysts



**Citation:** Barba, D.; Vaiano, V.; Palma, V. Selective Catalytic Oxidation of Lean-H<sub>2</sub>S Gas Stream to Elemental Sulfur at Lower Temperature. *Catalysts* **2021**, *11*, 746. <https://doi.org/10.3390/catal11060746>

Academic Editor: Stefano Cimino

Received: 28 May 2021

Accepted: 16 June 2021

Published: 18 June 2021

**Publisher's Note:** MDPI stays neutral with regard to jurisdictional claims in published maps and institutional affiliations.



**Copyright:** © 2021 by the authors. Licensee MDPI, Basel, Switzerland. This article is an open access article distributed under the terms and conditions of the Creative Commons Attribution (CC BY) license (<https://creativecommons.org/licenses/by/4.0/>).

## 1. Introduction

Hydrogen sulfide (H<sub>2</sub>S) is a common gas pollutant, which is harmful to human health with deleterious effects on many industrial catalysts, and represents the main source of acid rains when it is oxidized to sulfur dioxide (SO<sub>2</sub>) [1]. Many attempts have been focused on H<sub>2</sub>S removal from gaseous streams due to the worldwide increase in restrictive emission standards. Today, H<sub>2</sub>S-removal-based processes include wet scrubbing [2], biological methods [3], adsorption [4], and selective catalytic oxidation [5]. Among these purification processes, selective catalytic oxidation seems to be very promising for lean-H<sub>2</sub>S gas streams, where the concentration of hydrogen sulfide is in the range 0.1–10 vol%.

Typically, lean-H<sub>2</sub>S gas is characteristic of tail gas treating (<5 wt% H<sub>2</sub>S), crude petroleum (0.3–0.8 wt% H<sub>2</sub>S), and natural gas streams (0.03–0.3 wt% H<sub>2</sub>S), although in this last case the H<sub>2</sub>S can also reach 30 wt% [6].

The selective catalytic oxidation of H<sub>2</sub>S into elemental sulfur is one of the treatment methods employed for the removal of H<sub>2</sub>S from the Claus process tail gas [7,8]. This reaction can be performed above or below the sulfur dew point (180 °C) and the processes used are super-Claus, doxosulfreen (Elf-Lurgi), and the mobil direct oxidation process (MODOP) [9]. The super-Claus process, developed in 1985, is continuously being improved and allows achievement of a desulfurization efficiency of ~99.5% at 240 °C in the presence of iron- and chromium-based catalysts supported on alumina or silica [10]. In MODOP, the direct oxidation of H<sub>2</sub>S into elemental sulfur occurs on a TiO<sub>2</sub>-based catalyst that deactivates in the presence of water [11]. In the super-Claus process, H<sub>2</sub>S is oxidized without removing water from the tail gas. Metal-oxide-based catalysts, such as Al<sub>2</sub>O<sub>3</sub>, TiO<sub>2</sub>, V<sub>2</sub>O<sub>5</sub>, Mn<sub>2</sub>O<sub>3</sub>, Fe<sub>2</sub>O<sub>3</sub>, and CuO are the most used and investigated for H<sub>2</sub>S-selective catalytic oxidation [12]. Indeed, vanadium oxides have been investigated as active phases for H<sub>2</sub>S selective oxidation and are used as bulk V<sub>2</sub>O<sub>5</sub> [13], mixed with other metals [14], or supported over commercial [15] and mesoporous materials [16].

In our previous works, vanadium-based catalysts supported on different metal oxides ( $\text{CeO}_2$ ,  $\text{TiO}_2$ , and  $\text{CuFe}_2\text{O}_4$ ) were investigated for  $\text{H}_2\text{S}$  removal from biogas by partial and selective oxidation reactions in the temperature range 50–250 °C [17]. The optimization of the  $\text{V}_2\text{O}_5$  loading (2.55–50 wt%) was performed on the  $\text{CeO}_2$  support at the temperature of 150 °C [18]. The 20 wt%  $\text{V}_2\text{O}_5/\text{CeO}_2$  catalyst showed the best catalytic performance in terms of  $\text{H}_2\text{S}$  conversion (99%) and sulfur selectivity (99%) at 150 °C, by feeding a very diluted stream containing only 500 ppm of  $\text{H}_2\text{S}$  [19]. Structured catalysts starting from a cordierite carrier in the form of a monolith honeycomb were also prepared, characterized, and tested at low temperature and evidenced high activity and very low  $\text{SO}_2$  selectivity [20,21].

Based on these obtained promising results, in this study, vanadium-based catalysts supported on ceria were prepared, characterized, and tested in the presence of a lean- $\text{H}_2\text{S}$  gas stream containing a  $\text{H}_2\text{S}$  concentration higher than 5 vol%, which is a typical concentration of the Claus process tail gas. A preliminary screening of the catalysts with different vanadium loadings was carried out at 327 °C, in order to identify the catalyst formulation able to maximize the  $\text{H}_2\text{S}$  conversion and depress the  $\text{SO}_2$  formation in the presence of 10 vol% of  $\text{H}_2\text{S}$ . The effect of the main operating parameters, such as temperature, contact time, and  $\text{H}_2\text{S}$  inlet concentration, was also investigated.

## 2. Results and Discussion

### 2.1. Catalytic Activity Test

First of all, the reaction system was studied in the presence of 10 vol% of  $\text{H}_2\text{S}$  at the temperature of 327 °C without the catalyst (Figure 1).

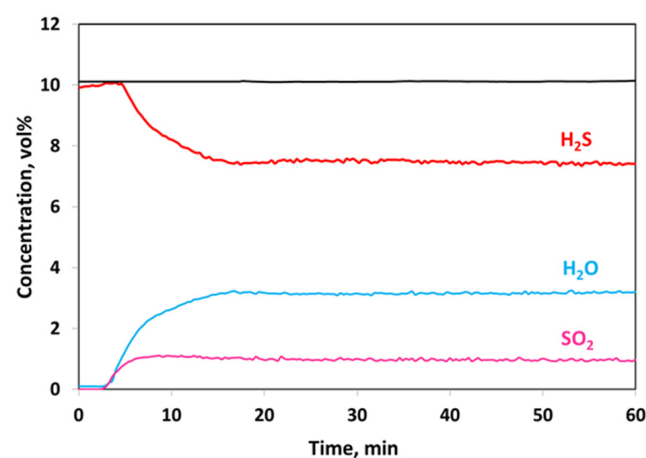


**Figure 1.** Activity test without catalyst ( $T = 327$  °C,  $\text{H}_2\text{S} = 10$  vol%, residence time = 0.6 s).

Figure 1 shows the behavior of  $\text{H}_2\text{S}$ ,  $\text{H}_2\text{O}$ , and  $\text{SO}_2$  during 1 h of time on stream.

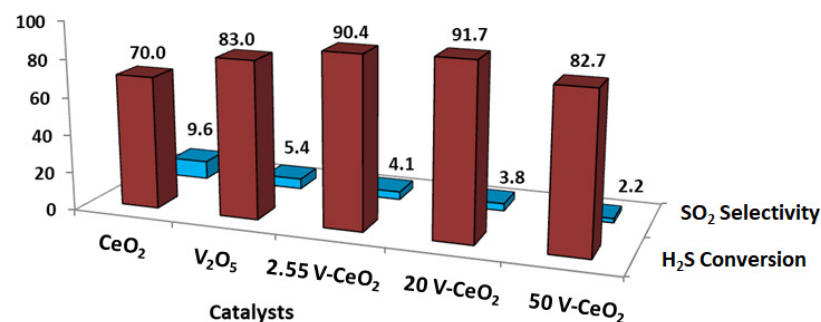
After the first 5 min, the feed stream was sent to the reactor and the formation of  $\text{SO}_2$  and water could be observed. The sulfur formation was not detectable because of the removal by the gaseous stream in the sulfur trap. The final  $\text{H}_2\text{S}$  conversion was 26%, while the  $\text{SO}_2$  selectivity was high enough (~39%). The  $\text{SO}_3$  formation ( $m/z = 80$ ) was not observed either for the test in the absence of a catalyst or for all the catalytic tests. In Table 1, the values obtained by the test carried out without the catalyst were compared with the ones expected by the thermodynamic equilibrium and with the experimental data achieved with 20 V- $\text{CeO}_2$  catalyst.

**Table 1.** Comparison between non-catalytic system, catalytic system, and equilibrium ( $T = 327\text{ }^{\circ}\text{C}$ ,  $\text{H}_2\text{S} = 10\text{ vol}\%$ ).

	No Catalyst	20 V-CeO <sub>2</sub>	Equilibrium
H <sub>2</sub> S Conversion, %	26 ( $\pm 1.5$ )	92 ( $\pm 1.5$ )	90
SO <sub>2</sub> Selectivity, %	38.5 ( $\pm 2$ )	4 ( $\pm 2$ )	6
SO <sub>2</sub> , vol%	1	0.4	0.5

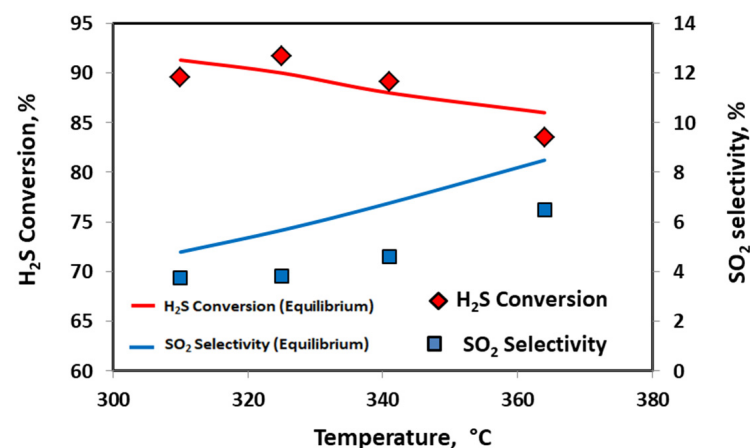
It is evident that the reaction system without the catalyst is very far from the equilibrium conditions; in fact, the expected H<sub>2</sub>S conversion and SO<sub>2</sub> concentration would be, respectively, 90% and 0.5 vol%. Conversely, the catalytic performance of the 20 V-CeO<sub>2</sub> sample is very close to that expected from the equilibrium, confirming the key role of the catalyst for maximizing the H<sub>2</sub>S conversion and inhibiting the SO<sub>2</sub> formation.

The screening of the vanadium-based catalysts was performed at 327 °C and the catalytic activity of the V-CeO<sub>2</sub> samples was also compared with the support (CeO<sub>2</sub>) and with the bulk V<sub>2</sub>O<sub>5</sub>. For each sample, the catalytic performance under steady-state conditions is reported in Figure 2.

**Figure 2.** Catalytic performance of the different catalysts under steady-state conditions ( $T = 327\text{ }^{\circ}\text{C}$ ,  $\text{H}_2\text{S} = 10\text{ vol}\%$ , contact time = 0.6 s).

The best catalytic performance can be observed for the catalysts having a V<sub>2</sub>O<sub>5</sub> loading of 2.55 and 20 wt%, for which the H<sub>2</sub>S conversion and SO<sub>2</sub> selectivity values are very similar. Although the lowest SO<sub>2</sub> selectivity (2.2%) was observed for the 50 V-CeO<sub>2</sub> sample, it unfortunately showed the lowest H<sub>2</sub>S conversion (83%).

The influence of the temperature was investigated for the 20 V-CeO<sub>2</sub> catalyst and the experimental data for H<sub>2</sub>S conversion and SO<sub>2</sub> selectivity were compared with the equilibrium data (red and blue lines, respectively) (Figure 3).

**Figure 3.** Temperature effect over 20 V-CeO<sub>2</sub> catalyst on the H<sub>2</sub>S conversion and SO<sub>2</sub> selectivity ( $\text{H}_2\text{S} = 10\text{ vol}\%$ , contact time = 0.6 s).

As it is possible to observe from Figure 3, the H<sub>2</sub>S conversion is very close to the equilibrium values (red line) while the SO<sub>2</sub> selectivity is, in the overall investigated temperature range, slightly below the equilibrium calculation (blue line), evidencing that the catalyst is able to inhibit the SO<sub>2</sub> formation. The effect of the H<sub>2</sub>S concentration, in the range 6–15 vol%, was then evaluated at the temperature of 327 °C (Figure 4).

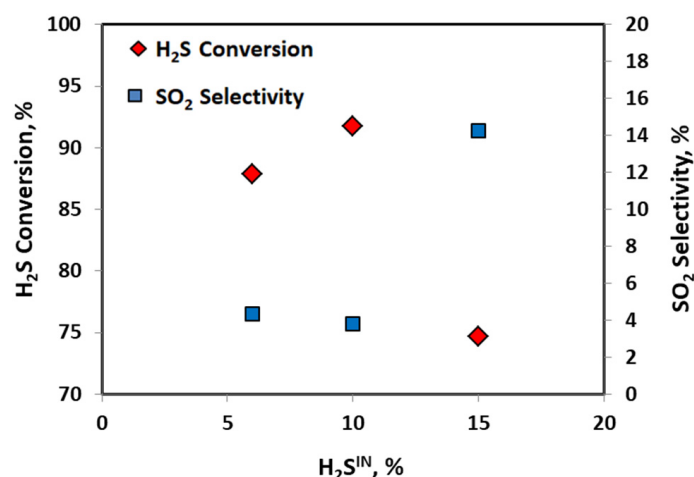


**Figure 4.** Influence of the H<sub>2</sub>S inlet concentration over 20 V-CeO<sub>2</sub> catalyst on the H<sub>2</sub>S conversion and SO<sub>2</sub> selectivity (O<sub>2</sub>/H<sub>2</sub>S = 0.5, T = 327 °C, contact time = 0.6 s).

The highest value of H<sub>2</sub>S conversion and the lowest SO<sub>2</sub> selectivity were observed when the H<sub>2</sub>S inlet concentration was 10 vol%. In the presence of a feed stream more concentrated in H<sub>2</sub>S (15 vol%), the conversion was drastically reduced to 75% and the SO<sub>2</sub> concentration was about 1.5 vol%; in this case, the selectivity increase is of one magnitude order (14%) with respect to the other obtained values. In Table 2, the equilibrium data are compared with those obtained experimentally at different H<sub>2</sub>S inlet concentrations.

**Table 2.** Equilibrium and experimental data by varying the H<sub>2</sub>S inlet concentration (T = 327 °C, contact time = 0.6 s).

H <sub>2</sub> S <sup>IN</sup> , vol%	xH <sub>2</sub> S, %	xH <sub>2</sub> S Eq., %	S SO <sub>2</sub> , %	sSO <sub>2</sub> Eq., %
6	88 (±1.5)	89	4.4 (±2)	4
10	92 (±1.5)	90	4 (±2)	6
15	75 (±1.5)	90	14 (±2)	9

Based on the data listed in Table 2, it is possible to see that the reaction system deviates from the equilibrium values especially in presence of 15 vol% of H<sub>2</sub>S.

The influence of the contact time on the catalytic performance is reported in Figure 5. For comparison, the equilibrium data for both H<sub>2</sub>S conversion and SO<sub>2</sub> selectivity at the temperature of 327 °C are also shown.

The catalytic performance resulted in little affected from the variation of the contact time. In particular, it is noteworthy to evidence that the H<sub>2</sub>S conversion is quite close to the equilibrium values, while the SO<sub>2</sub> selectivity is in all cases below the equilibrium value.

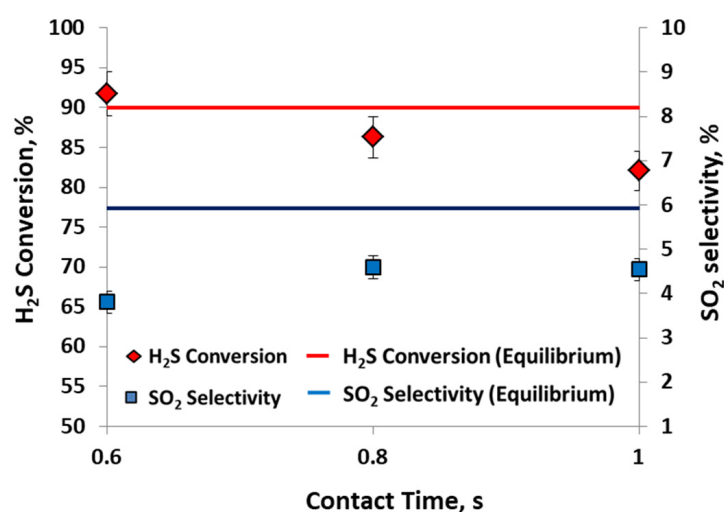


**Figure 5.** Effect of the contact time over 20 V-CeO<sub>2</sub> catalyst on the H<sub>2</sub>S conversion and SO<sub>2</sub> selectivity (T = 327 °C, H<sub>2</sub>S = 10 vol%).

## 2.2. Catalyst Characterization

The nominal and measured vanadium oxide content of the catalysts before the activation step is reported in Table 3.

**Table 3.** Theoretical and measured vanadium content of the catalysts before the sulfuration.

Sample	V <sub>2</sub> O <sub>5</sub> Nominal wt%	% V <sub>2</sub> O <sub>5</sub> Measured wt%
2.55 V-CeO <sub>2</sub>	2.55	2.7
20 V-CeO <sub>2</sub>	20	22
50 V-CeO <sub>2</sub>	50	51

The results reported evidence that the nominal V<sub>2</sub>O<sub>5</sub> loading is very close to the measured loading.

The specific surface areas of the fresh and used catalysts are reported in Table 4.

**Table 4.** Specific surface area (SSA, m<sup>2</sup>/g) of the fresh and used catalysts.

Sample	CeO <sub>2</sub>	V <sub>2</sub> O <sub>5</sub>	2.55 V-CeO <sub>2</sub>	20 V-CeO <sub>2</sub>	50 V-CeO <sub>2</sub>
Fresh	29	8	25	22	20
Used	17	2	17	4	14

The lowest SSA was observed for the sample that was not supported (V<sub>2</sub>O<sub>5</sub>). In particular, the value of bulk V<sub>2</sub>O<sub>5</sub> (8 m<sup>2</sup>/g) decreased more than 50% after the catalytic test. For the fresh V-CeO<sub>2</sub> catalysts, the values of SSA were slightly lower than the CeO<sub>2</sub> support (~30 m<sup>2</sup>/g). After the catalytic activity tests, the SSA decrease was likely due to the sulfur deposition on the catalyst surface. This aspect was more evident for the 20 V-CeO<sub>2</sub> sample (SSA = 4 m<sup>2</sup>/g) and was confirmed by XRD and Raman characterizations.

Raman spectra of the support and fresh catalysts are shown in Figure 6. The Raman spectrum for pure CeO<sub>2</sub> shows the main band at 460 cm<sup>-1</sup>, ascribable to ceria in the typical cubic crystal structure of fluorite-type cerium oxide [22,23]. The 2.55 V-CeO<sub>2</sub> sample shows that such Raman band slightly shifted to 465 cm<sup>-1</sup>, while in the case of the catalysts with the highest V loading this band shifted up to 454 cm<sup>-1</sup>. A more detailed discussion of these results is reported in the Supplementary Materials (Figure S1).

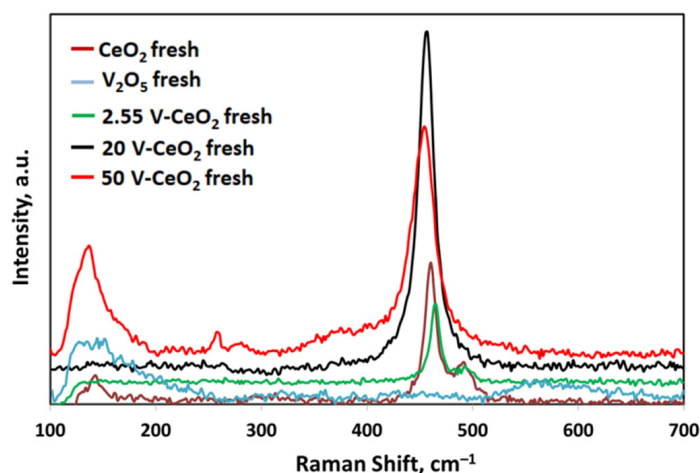


Figure 6. Raman spectra of  $\text{CeO}_2$ ,  $\text{V}_2\text{O}_5$ , and 2.55, 20, 50 V- $\text{CeO}_2$  fresh catalysts.

The XRD spectra of  $\text{CeO}_2$  and the fresh catalysts are shown in Figure 7. All the catalysts exhibit the characteristic peaks of  $\text{CeO}_2$  at  $28.3^\circ$ ,  $32.8^\circ$ ,  $47.3^\circ$ ,  $56.1^\circ$ ,  $58^\circ$ , and  $69^\circ$ , corresponding to diffraction planes indexed as (1 1 1), (2 0 0), (2 2 0), (3 1 1), (2 2 2), and (4 0 0), respectively [24]. These patterns are ascribable to the typical cubic crystal structure of fluorite-type cerium oxide [25]. No additional reflections attributable to  $\text{V}_2\text{O}_5$  are detectable, evidencing that the sulfuration of the catalysts completely occurred [26]. Furthermore, there were no peaks detected that related to typical vanadium sulfides ( $\text{VS}_2$ ,  $\text{VS}_4$ ,  $\text{V}_2\text{S}_3$ ,  $\text{V}_3\text{S}_4$ ) that might have formed following the sulfuration treatment [27].

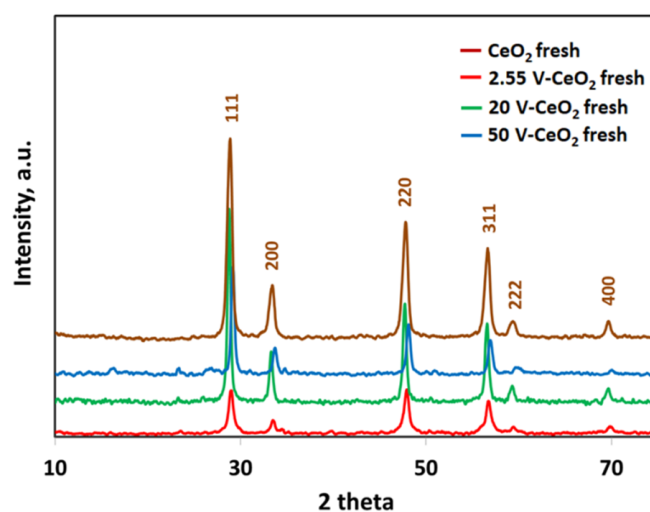
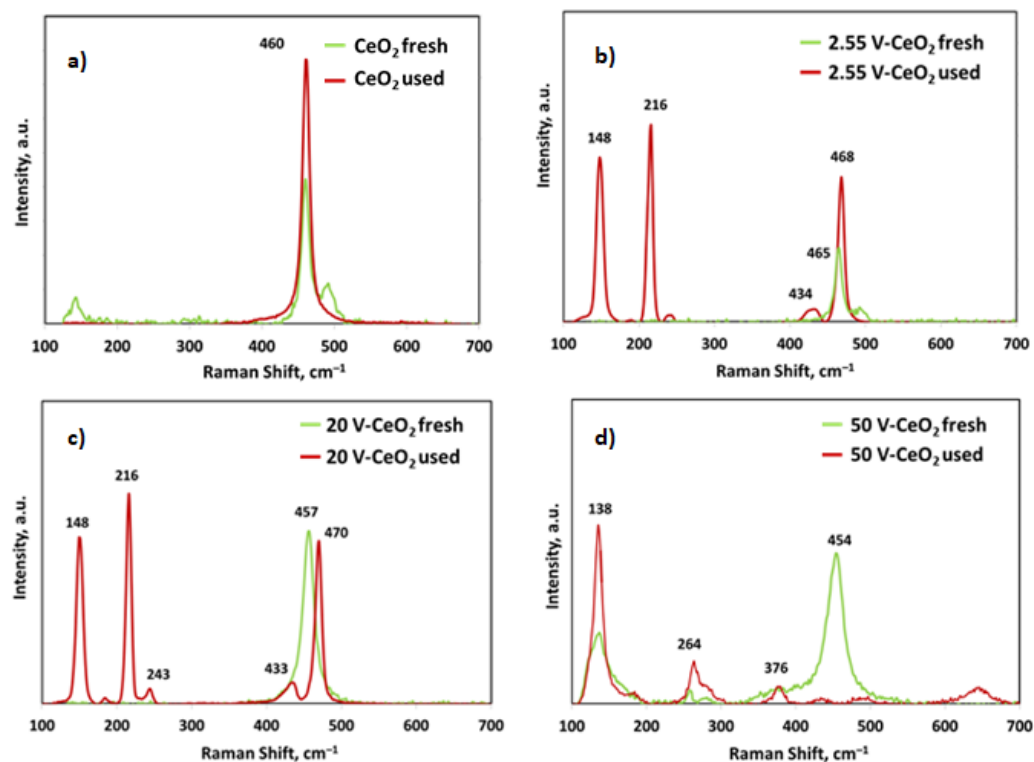


Figure 7. XRD spectra of  $\text{CeO}_2$  and 2.55, 20, 50 V- $\text{CeO}_2$  fresh catalysts.

In Figure 8, the Raman spectra of the fresh samples ( $\text{CeO}_2$  and V- $\text{CeO}_2$  catalysts) are compared with the used catalysts. The used  $\text{CeO}_2$ , equally to the fresh one, has the characteristic Raman peak perfectly centered at  $460\text{ cm}^{-1}$  (Figure 8a) [22,23]. A slight shift of this Raman band up to  $465\text{ cm}^{-1}$ ,  $457\text{ cm}^{-1}$ , and  $454\text{ cm}^{-1}$  (Figure 8b–d) is detectable for 2.55 V- $\text{CeO}_2$ , 20 V- $\text{CeO}_2$ , and 50 V- $\text{CeO}_2$  fresh catalysts, respectively, as already previously observed (Figure 6). A detailed discussion of the Raman results is reported in the Supplementary Materials (Figure S2).



**Figure 8.** Raman spectra of fresh and used catalysts: CeO<sub>2</sub> (a), 2.55 V-CeO<sub>2</sub> (b), 20 V-CeO<sub>2</sub> (c), 50 V-CeO<sub>2</sub> (d).

Furthermore, the absence of any characteristic bands of the vibrational modes of crystalline V<sub>2</sub>O<sub>5</sub> [28] and V = O stretching vibration ascribable to monovanadate species (VO<sub>4</sub><sup>3-</sup>) denotes that the sulfuration of the catalysts occurred completely [16]. The Raman spectrum of the bulk V<sub>2</sub>O<sub>5</sub> after the catalytic test is reported in Figure 9.

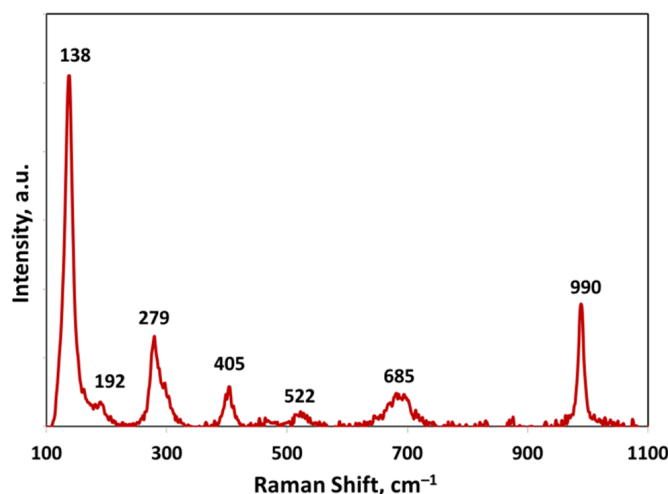


**Figure 9.** Raman spectra of V<sub>2</sub>O<sub>5</sub> used.

The Raman bands at 140, 192, 282, 405, 688, and 993 cm<sup>-1</sup> are characteristic of the vanadium sulfide in VS<sub>2</sub> form, as reported in the literature [29]. In particular, all the signals correspond to the rocking combination and stretching vibrations of V-S bonds or their combination [30]. Moreover, no bands related to the formation of vanadyl sulfate (984 cm<sup>-1</sup> and 1060 cm<sup>-1</sup>) were observed [31].

In Figure 10, the XRD patterns of the fresh samples are compared with the used ones. There are no differences between the XRD spectra of the fresh/used bulk CeO<sub>2</sub>; for the used

sample less intensity of the peaks is observed, which is likely due to the sulfur deposition (Figure 10a). For the used 2.55 V-CeO<sub>2</sub> catalyst, in addition to the characteristic peaks of the CeO<sub>2</sub> fresh sample, a signal is visible at  $2\theta = 23^\circ$  due to the sulfur formation [32], as also confirmed from Raman analysis (Figure 10b). The spectra of the used 20 V-CeO<sub>2</sub> catalyst (Figure 10c) are different, where other peaks attributable to the sulfur are observable at  $2\theta = 23^\circ, 24^\circ, 26^\circ, 27^\circ,$  and  $28^\circ$  [32]. For the 50 V-CeO<sub>2</sub> catalyst, the XRD spectrum of the fresh sample is perfectly stackable with that of the used sample (Figure 10d) because all the peaks are ascribable only to the CeO<sub>2</sub> support.

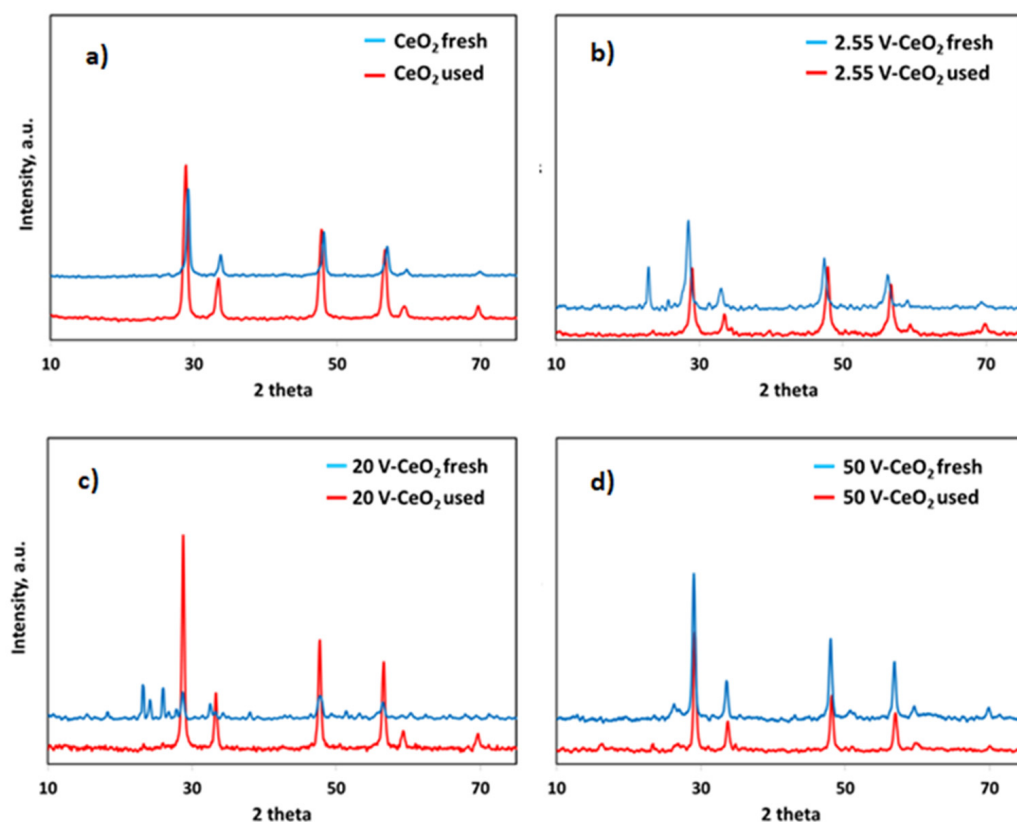


**Figure 10.** XRD spectra of fresh and used catalysts: CeO<sub>2</sub> (a), 2.55 V-CeO<sub>2</sub> (b), 20 V-CeO<sub>2</sub> (c), 50 V-CeO<sub>2</sub> (d).

The average crystallite size of ceria for the different catalysts, calculated with the Scherrer equation, are listed in Table 5.

**Table 5.** Average crystallite size ( $\langle L \rangle$ , nm) of the fresh and used catalysts.

Sample	Fresh	Used
CeO <sub>2</sub>	13	21
2.55 V-CeO <sub>2</sub>	16	19
20 V-CeO <sub>2</sub>	18	19
50 V-CeO <sub>2</sub>	24	25

As it is possible to observe from Table 5, the increase of the V-loading for the different catalysts has involved an increase in the crystallite size of the CeO<sub>2</sub>, as reported in the literature for supported vanadium catalysts [25]. The average crystallite size of bulk CeO<sub>2</sub> before the catalytic tests was 13 nm; it increased to 24 nm for the catalyst having the highest V-content (50 V-CeO<sub>2</sub>). Relatively to the catalysts, there is a negligible variation of the ceria average crystallite size between fresh and used samples.

The only significant variation between fresh and used samples was obtained for the support; the greater segregation of the CeO<sub>2</sub> after the catalytic activity tests involved the increase of the crystallite dimension (21 nm). The segregation of the CeO<sub>2</sub> crystallite may be due to the high SO<sub>2</sub> formation observed on the support in the absence of the active phase; in fact, among the catalysts, the highest value of SO<sub>2</sub> selectivity (~10%) was obtained for the CeO<sub>2</sub> at 327 °C as previously reported in Figure 2. The reaction temperature could favor the formation of sulfate species and also the oxygen in the ceria lattice could facilitate the CeO<sub>2</sub> sulfuration [33]; therefore, the reaction between CeO<sub>2</sub> and SO<sub>2</sub> could occur, leading to the formation of cerium sulfate Ce(SO<sub>4</sub>)<sub>2</sub>, which is stable at high temperature and decomposes between 722 and 843 °C to CeO<sub>2</sub> [34].

### 3. Materials and Methods

#### 3.1. Catalyst Preparation and Characterization

The preparation of vanadium-based catalysts supported on ceria with different loading of active phase (2.55, 20, and 50 wt% V<sub>2</sub>O<sub>5</sub> nominal loading) was described in detail in our previous work [19]. All the reactants were provided by Sigma Aldrich. After the calcination, the sulfuration procedure was carried out in a quartz reactor containing the catalyst to be sulfurized. In particular, the activation step was realized by feeding a gaseous stream containing N<sub>2</sub> and H<sub>2</sub>S at 20 vol%, by increasing the temperature from ambient temperature up to 200 °C with a heating rate of 10 °C/min for 1 h. Finally, the catalysts were reduced to the size 38–180 µm. For simplicity, the catalysts are named in the paper as follows: 2.55 V-CeO<sub>2</sub>, 20 V-CeO<sub>2</sub>, 50 V-CeO<sub>2</sub>, where “2.55” means the nominal V loading (wt%) expressed as V<sub>2</sub>O<sub>5</sub>. The sulfurized samples before the testing are named “fresh”, while they are named “used” after the catalytic activity test.

The catalysts were characterized by nitrogen adsorption at 77 K, Raman spectroscopy and X-ray diffraction. The specific surface area was evaluated with a Costech Sorptometer 1040 (Costech International, Firenze, Italy) by using N<sub>2</sub> and He, respectively, as adsorptive and carrier gas. The powder catalysts were treated at 150 °C for 30 min in a He flow prior to testing. A BET method multipoint analysis based on N<sub>2</sub> adsorption/desorption isotherms at 77 K was used to evaluate the specific surface area of the fresh and used catalysts. X-ray diffraction (XRD) was performed using a Bruker D2 Phaser (Germany) using CuKα radiation (λ = 1.5401 Å). Laser Raman spectra of the catalysts were obtained in air with a Dispersive MicroRaman (Invia, Renishaw, Italy), equipped with a 514 nm diode-laser, in the range of 100–2000 cm<sup>-1</sup> Raman shift. The V-content of the fresh catalysts (expressed as V<sub>2</sub>O<sub>5</sub> wt%) was evaluated by X-ray fluorescence (XRF) spectra by using an ARL QUANT'X EDXRF spectrometer (ThermoFisher Scientific, Italy).

#### 3.2. Experimental Apparatus

The catalytic activity tests were performed in the laboratory plant schematized in Figure 11.

The laboratory plant is made of three sections: feed, reaction, and analysis sections. The feed stream containing H<sub>2</sub>S, O<sub>2</sub>, and N<sub>2</sub> is sent by a three-way valve to the reactor, or in bypass position to the analyzer to verify the composition. All gases came from SOL S.p.A with a purity degree of 99.999% for N<sub>2</sub>, O<sub>2</sub>, and SO<sub>2</sub>, and 99.5% for H<sub>2</sub>S.

The reaction system comprises a furnace, a reactor, and a sulfur abatement trap. The quartz-made reactor, consisting of a tube of 300 mm length and an internal diameter of 19 mm, is housed in a vertical furnace heated with silicon carbide (SiC)-based resistances. At the bottom of the reactor are a reactant inlet and a thermocouple sheet concentric to the reactor. The catalytic bed is placed in the isothermal zone of the reactor and the temperature is measured continuously by a K-type thermocouple. In the head of the reactor is welded a trap for the sulfur abatement, which is made of an expansion vessel that allows the sulfur to liquefy, involving its separation by the gaseous stream. This trap is maintained at the temperature of 250 °C.

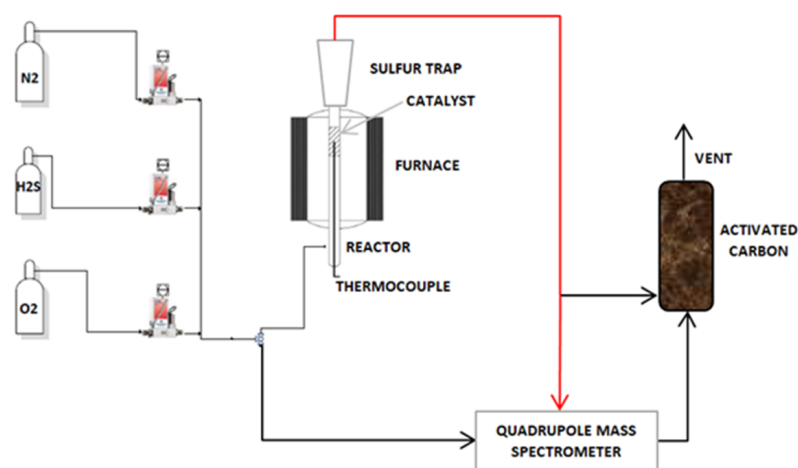


**Figure 11.** Scheme of the apparatus plant.

All the lines downstream of the reactor were heated at the temperature of 170 °C to avoid sulfur solidification and possible clogging of the mass spectrometer capillary and to maintain the water in the gas phase for the analysis. The analysis of the gaseous stream ( $\text{H}_2\text{S}$ ,  $\text{O}_2$ ,  $\text{N}_2$ ,  $\text{SO}_2$ ,  $\text{SO}_3$ ) was performed with the mass spectrometer quadrupole (Hiden HPR-20) (Warrington, United Kingdom).

Finally, the abatement of unconverted  $\text{H}_2\text{S}$  was realized by adsorption on activated carbons loaded in a special vessel having a capacity of 10 Lt. Furthermore, the entire apparatus plant was housed under the hood and isolated from the external environment in order to avoid gas leakage.

The operating conditions of the catalytic activity tests are listed in Table 6.

**Table 6.** Operating conditions.

Operating Conditions	
Temperature	200–367 °C
Contact Time	0.6–1 s
Catalyst Volume	3 cm <sup>3</sup>
Total Flow Rate	180–300 Ncc·min <sup>-1</sup>
GHSV	3600–6000 h <sup>-1</sup>
$\text{H}_2\text{S}^{\text{IN}}$ concentration	6–15 vol%
$\text{O}_2/\text{H}_2\text{S}$	0.5

$\text{H}_2\text{S}$  conversion ( $x \text{H}_2\text{S}$ ) and the  $\text{SO}_2$  selectivity ( $s \text{SO}_2$ ) were calculated by using the following relationship (Equations (1) and (2)), by considering the gas phase volume change to be negligible:

$$x \text{H}_2\text{S}, \% = ((\text{H}_2\text{S}^{\text{IN}} - \text{H}_2\text{S}^{\text{OUT}}) / \text{H}_2\text{S}^{\text{IN}}) \cdot 100 \quad (1)$$

$$s \text{SO}_2, \% = (\text{SO}_2^{\text{OUT}} / (\text{H}_2\text{S}^{\text{IN}} - \text{H}_2\text{S}^{\text{OUT}})) \cdot 100 \quad (2)$$

For the equilibrium calculation, the *GasEq* program was used, software (0.7.0.9 version, Chris Morley) based on the minimization of Gibbs free energy, which is able to calculate the equilibrium product composition of an ideal gaseous mixture when there are a lot of simultaneous reactions. The thermodynamic analysis was carried out considering the following chemical species that could be present at equilibrium:  $\text{H}_2\text{S}$ ,  $\text{O}_2$ ,  $\text{SO}_2$ ,  $\text{S}_2$ ,  $\text{S}_6$ ,  $\text{S}_8$ ,  $\text{H}_2\text{O}$ , and nitrogen.

#### Calibration Procedure

The calibration procedure is required in order to measure the concentration of all the species that could be in the gas stream for analysis and, for this reason, it must be performed prior to carrying out experimental tests. However, it could be necessary to repeat

the calibration every time the process conditions are changed (e.g., after the replacement of the capillary, the filaments, change of pressure chamber value) or when the signal seems to be affected by derivative effects. The measurements could be affected by interference due to the presence of ions of different molecules having the same  $m/z$  ratio. Each molecule has a matrix of interference, which defines the “weight” of the disturbance of other molecules on the partial pressure of the molecule in the phase of calibration. The partial pressure obtained, net of the relative interference, must be corrected by a response factor, thus returning the actual partial pressure of each molecule in the stream analyzed. At this point, it is possible to calculate the correct concentration of each component. The calibration procedure is characterized by different steps:

- (1) Report in a table the partial pressure of the all-mass fragment for each concentration of the component to calibrate;
- (2) Construct the matrix of interference and the response factors table relatively for the component you are calibrating;
- (3) Calculate the concentrations of the component calibrated by considering the relative interference of other species on the component to calibrate and correcting the measure by its response factor.

After the calibration, which is carried out in a by-pass position, the feed stream can be sent to the reactor. The reactor, before each test, is purged with nitrogen to avoid humidity and/or impurity and is heated up to the reaction temperature at which the feed stream is sent.

Similarly, at the end of the activity test, the reactor is cooled down with nitrogen to room temperature.

#### 4. Conclusions

The  $H_2S$  selective oxidation reaction to sulfur and water was investigated over vanadium-sulfide-based catalysts supported on  $CeO_2$ . The catalysts were prepared with different vanadium loading and were characterized before and after the catalytic tests with different techniques. X-ray diffraction and Raman analysis showed a good dispersion of the V-species on the support because the V-sulfide presence was not detected on the different catalysts. The only vanadium sulfide in  $VS_2$  form was observed for the bulk  $V_2O_5$  after the catalytic tests. Furthermore, the presence of the sulfur was observed especially over the used catalysts at lower V-loading by Raman and SSA analysis.

From the preliminary screening of the catalysts performed at 327 °C, the higher catalytic activity was observed over the 2.55 V- $CeO_2$  and 20 V- $CeO_2$  catalysts, with  $H_2S$  conversion, respectively, of 90% and 92%, and  $SO_2$  selectivity of ~4%. No  $SO_3$  formation and catalyst deactivation phenomena by the sulfur deposition were observed. The effect of the temperature, contact time, and  $H_2S$  inlet concentration was studied over 20 V- $CeO_2$  catalysts. By increasing the  $H_2S$  inlet concentration (up to 15 vol%), the conversion decreased from 86% to 75% with an  $SO_2$  concentration of about 1.5 vol%. The effect of the contact time was almost negligible on the  $H_2S$  conversion and  $SO_2$  selectivity, while the temperature had a significant influence. In the range of temperatures investigated (300–370 °C), the  $H_2S$  conversion was very close to the equilibrium values while the  $SO_2$  selectivity was below the equilibrium calculation, evidencing that the catalyst is effectively able to inhibit  $SO_2$  formation.

Based on the obtained results, the ceria-supported vanadium catalysts could be considered good candidates to carry out the selective oxidation of  $H_2S$  to sulfur by an  $H_2S$ -lean gas stream (e.g., natural gas, Claus process tail gas) at very low temperature.

**Supplementary Materials:** The following are available online at <https://www.mdpi.com/article/10.3390/catal11060746/s1>: Figure S1: Raman Spectra of  $CeO_2$ ,  $V_2O_5$  and 2.55, 20, 50 V- $CeO_2$  fresh catalysts; Figure S2: Raman Spectra of fresh and used catalysts  $CeO_2$  (a), 2.55 V- $CeO_2$  (b), 20 V- $CeO_2$  (c), 50 V- $CeO_2$  (d).

**Author Contributions:** Conceptualization, D.B. and V.V.; methodology, D.B.; software, D.B.; validation, D.B. and V.V.; formal analysis, V.P.; investigation, D.B.; resources, V.V. and V.P.; data curation, V.P.; writing—original draft preparation, D.B.; writing—review and editing, V.V.; visualization, V.P. and V.V.; supervision, V.P.; project administration, D.B.; funding acquisition, V.P. All authors have read and agreed to the published version of the manuscript.

**Funding:** This research received no external funding.

**Conflicts of Interest:** The authors declare no conflict of interest.

## References

1. Forzatti, P.; Lietti, L. Catalyst deactivation. *Catal. Today* **1999**, *52*, 165–181. [[CrossRef](#)]
2. Wang, R. Investigation on a new liquid redox method for H<sub>2</sub>S removal and sulfur recovery with heteropoly compound. *Sep. Purif. Technol.* **2003**, *31*, 111–121. [[CrossRef](#)]
3. Duan, H.; Yan, R.; Koe, L.C.; Wang, X. Combined effect of adsorption and biodegradation of biological activated carbon on H<sub>2</sub>S biotrickling filtration. *Chemosphere* **2007**, *66*, 1684–1691. [[CrossRef](#)]
4. Seredych, M.; Bandoz, T.J. Sewage sludge as a single precursor for development of composite adsorbents/catalysts. *Chem. Eng. J.* **2007**, *128*, 59–67. [[CrossRef](#)]
5. Yasyerli, S.; Dogu, G.; Ar, I.; Dogu, T. Dynamic analysis of removal and selective oxidation of H<sub>2</sub>S to elemental sulfur over Cu–V and Cu–V–Mo mixed oxides in a fixed bed reactor. *Chem. Eng. Sci.* **2004**, *59*, 4001–4009. [[CrossRef](#)]
6. Elmawgoud, H.A.; Elshiekh, M.; Abdelkreem, M.; Khalil, S.A.; Alsabagh, A.M. Optimization of petroleum crude oil treatment using hydrogen sulfide scavenger. *Egypt. J. Pet.* **2019**, *28*, 161–164. [[CrossRef](#)]
7. Pi, J.H.; Lee, D.H.; Lee, J.D.; Jun, J.H.; Park, N.K.; Ryu, S.O.; Lee, T.J. The study on the selective oxidation of H<sub>2</sub>S over the mixture zeolite NaX-WO<sub>3</sub> catalysts. *Korean J. Chem. Eng.* **2004**, *21*, 126–131. [[CrossRef](#)]
8. Lee, J.D.; Han, G.B.; Park, N.K.; Ryu, S.O.; Lee, T.J. The selective oxidation of H<sub>2</sub>S on V<sub>2</sub>O<sub>5</sub>/zeolite-X catalysts in an IGCC system. *J. Ind. Eng. Chem.* **2006**, *12*, 80–85.
9. Wiheeb, A.D.; Shamsudin, I.K.; Ahmad, M.A.; Murat, N.M.; Kim, J.; Othman, M.R. Present technologies for hydrogen sulfide removal from gaseous mixtures. *Rev. Chem. Eng.* **2013**, *29*, 449–470. [[CrossRef](#)]
10. Keller, N.; Pham-Huu, C.; Crouzet, C.; Ledoux, M.J.; Savin-Poncet, S.; Nougayrede, J.B.; Bousquet, J. Direct oxidation of H<sub>2</sub>S into S: New catalysts and processes based on SiC support. *Catal. Today* **1999**, *53*, 535–542. [[CrossRef](#)]
11. Zhang, X.; Tang, Y.; Qu, S.; Da, J.; Hao, Z. H<sub>2</sub>S-selective catalytic oxidation: Catalysts and processes. *ACS Catal.* **2015**, *5*, 1053–1067. [[CrossRef](#)]
12. Davydov, A.A.; Marshneva, V.I.; Shepotko, M.L. The comparison study of the catalytic activity. Mechanism of the interactions between H<sub>2</sub>S and SO<sub>2</sub> on some oxides. *Appl. Catal. A* **2003**, *244*, 93–100. [[CrossRef](#)]
13. Li, K.T.; Hyang, M.Y.; Cheng, W.D. Vanadium-based mixed-oxide catalysts for selective oxidation of hydrogen sulfide to sulfur. *Ind. Eng. Chem. Res.* **1996**, *35*, 621–626. [[CrossRef](#)]
14. Park, D.W.; Byung, B.H.; Ju, W.D.; Kim, M.I.; Kim, K.H.; Woo, H.C. Selective oxidation of hydrogen sulfide containing excess water and ammonia over Bi-V-Sb-O catalysts. *Korean J. Chem. Eng.* **2005**, *22*, 190–195. [[CrossRef](#)]
15. Kalinkin, P.; Kovalenko, O.; Lapina, O.; Khabibulin, D.; Kundo, N. Kinetic peculiarities in the low-temperature oxidation of H<sub>2</sub>S over vanadium catalysts. *J. Mol. Catal. A Chem.* **2002**, *178*, 173–180. [[CrossRef](#)]
16. Soriano, M.D.; Jimenez-Jimenez, J.; Concepcion, P.; Jimenez-Lopez, A.; Rodriguez-Castellon, E.; Lopez Nieto, J.M. Selective oxidation of H<sub>2</sub>S to sulfur over vanadia supported on mesoporous zirconium phosphate heterostructure. *Appl. Catal. B Environ.* **2009**, *92*, 271–279. [[CrossRef](#)]
17. Palma, V.; Barba, D.; Ciambelli, P. Screening of catalysts for H<sub>2</sub>S abatement from biogas to feed molten carbonate fuel cells. *Int. J. Hydrogen Energy* **2013**, *38*, 328–335. [[CrossRef](#)]
18. Palma, V.; Barba, D. Low temperature catalytic oxidation of H<sub>2</sub>S over V<sub>2</sub>O<sub>5</sub>/CeO<sub>2</sub> catalysts. *Int. J. Hydrogen Energy* **2014**, *39*, 21524–21530. [[CrossRef](#)]
19. Palma, V.; Barba, D. Vanadium-ceria catalysts for H<sub>2</sub>S abatement from biogas to feed to MCFC. *Int. J. Hydrogen Energy* **2017**, *42*, 1891–1898. [[CrossRef](#)]
20. Palma, V.; Barba, D.; Gerardi, V. Honeycomb-structured catalysts for the selective partial oxidation of H<sub>2</sub>S. *J. Clean Prod.* **2016**, *111*, 69–75. [[CrossRef](#)]
21. Palma, V.; Barba, D. Honeycomb V<sub>2</sub>O<sub>5</sub>-CeO<sub>2</sub> catalysts for H<sub>2</sub>S abatement from biogas by direct selective oxidation to sulfur at low temperature. *Chem. Eng. Trans.* **2015**, *43*, 1957–1962. [[CrossRef](#)]
22. Gu, X.; Ge, J. Structural, redox and acid–base properties of V<sub>2</sub>O<sub>5</sub>/CeO<sub>2</sub> catalyst. *Thermochim. Acta* **2006**, *451*, 84–93. [[CrossRef](#)]
23. Escribano, V.S.; López, E.F.; Panizza, M.; Resini, C.; Amores, J.M.G.; Busca, G. Characterization of cubic ceria–zirconia powders by X-ray diffraction and vibrational and electronic spectroscopy. *Solid State Sci.* **2003**, *5*, 1369–1376. [[CrossRef](#)]
24. Sun, C.; Li, H.; Zhang, H.; Wang, Z.; Chen, L. Controlled synthesis of CeO<sub>2</sub> nanorods by a solvothermal method. *Nanotechnology* **2005**, *16*, 1454–1463. [[CrossRef](#)]
25. Radhika, T.; Sugunan, S. Structural and catalytic investigation of vanadia supported on ceria promoted with high surface area rice husk silica. *J. Mol. Catal. A Chem.* **2006**, *250*, 169–176. [[CrossRef](#)]

26. Singh, B.; Gupta, M.K.; Mishra, S.K.; Mittal, R.; Sastry, P.U.; Rolsc, S.; Lal Chaplot, S. Anomalous lattice behavior of vanadium pentaoxide ( $V_2O_5$ ): X-ray diffraction, inelastic neutron scattering and ab initio lattice dynamics. *Phys. Chem. Chem. Phys.* **2017**, *19*, 17967. [[CrossRef](#)]
27. Liu, Y.Y.; Xu, L.; Guo, X.T.; Lv, T.T.; Pang, H. Vanadium sulfide based materials: Synthesis, energy storage and conversion. *J. Mater. Chem.* **2020**, *8*, 20781–20802. [[CrossRef](#)]
28. Holgado, J.P.; Soriano, M.D.; Jimenez, J. Operando XAS and Raman study on the structure of a supported vanadium 409 oxide catalyst during the oxidation of H<sub>2</sub>S to sulfur. *Appl. Catal. B* **2010**, *92*, 271–279, 410. [[CrossRef](#)]
29. Huang, L.; Zhu, W.; Zhang, W.; Chen, K.; Wang, J.; Wang, R.; Yang, Q.; Hu, N.; Suo, Y.; Wang, J. Layered vanadium (IV) 414 disulfide nanosheets as a peroxidase-like nanozyme for colorimetric detection of glucose. *Microchim. Acta* **2018**, *185*, 415. [[CrossRef](#)]
30. Qu, Y.; Shao, M.; Shao, Y.; Yang, M.; Xu, J.; Kwok, C.T.; Shi, X.; Lu, Z.; Pan, H. Ultra-high electrocatalytic activity of VS<sub>2</sub> nanoflowers for efficient hydrogen evolution reaction. *J. Mater. Chem. A* **2017**, *5*, 15080–15086. [[CrossRef](#)]
31. Evans, J.C. The vibrational spectra and structure of the vanadyl ion in aqueous solution. *Inorg. Chem.* **1963**, *2*, 372–375. [[CrossRef](#)]
32. Xu, J.; Su, D.; Zhang, W.; Bao, W.; Wang, G. A nitrogen–sulfur co-doped porous graphene matrix as a sulfur immobilizer for high performance lithium–sulfur batteries. *J. Mater. Chem. A* **2016**, *4*, 17381–17393. [[CrossRef](#)]
33. Smirnov, M.Y.; Kalinkin, A.V.; Pashis, A.V.; Sorokin, A.M. Interaction of Al<sub>2</sub>O<sub>3</sub> and CeO<sub>2</sub> Surfaces with SO<sub>2</sub> and SO<sub>2</sub> + O<sub>2</sub> studied by X-ray photoelectron spectroscopy. *J. Phys. Chem. B* **2005**, *109*, 11712–11719. [[CrossRef](#)] [[PubMed](#)]
34. Sharma, I.B.; Singh, V.; Lakhanpal, M. Study of thermal decomposition of ammonium cerium sulphate. *J. Therm.* **1992**, *38*, 1345–1355. [[CrossRef](#)]